IOP Publishing Phys. Med. Biol. 63 (2018) 235023 (11pp) https://doi.org/10.1088/1361-6560/aaef16

Physics in Medicine & Biology

IPEM Institute of Physics and Engineering in Medicine

RECEIVED
9 August 2018

REVISED
1 November 2018

ACCEPTED FOR PUBLICATION
7 November 2018

PUBLISHED
4 December 2018

PAPER

Mechanical decellularization of tissue volumes using boiling histotripsy

Yak-Nam Wang[1], Tatiana D Khokhlova[2,9,10], Sergey Buravkov[3], Valeriy Chernikov[4], Wayne Kreider[1], Ari Partanen[5], Navid Farr[6], Adam Maxwell[7], George R Schade[7] and Vera A Khokhlova[1,8]

[1] Center for Industrial and Medical Ultrasound, Applied Physics Laboratory, University of Washington, Seattle, WA, United States of America
[2] Division of Gastroenterology, Department of Medicine, University of Washington, Seattle, WA, United States of America
[3] Faculty of Fundamental Medicine, M V Lomonosov Moscow State University, Moscow, Russia
[4] Research Institute of Human Morphology, Moscow, Russia
[5] Profound Medical Inc., Mississauga, Canada
[6] Department of Bioengineering, University of Washington, Seattle, WA, United States of America
[7] Department of Urology, University of Washington, Seattle, WA, United States of America
[8] Physics Faculty, M V Lomonosov Moscow State University, Moscow, Russia
[9] Box 359773, 325 Ninth Avenue, Seattle, WA 98104, United States of America
[10] Author to whom any correspondence should be addressed.

E-mail: tdk7@uw.edu

Keywords: high intensity focused ultrasound, HIFU, boiling histotripsy, tissue disintegration, decellularization, soft tissue scaffold

Abstract

High intensity focused ultrasound (HIFU) is rapidly advancing as an alternative therapy for non-invasively treating specific cancers and other pathological tissues through thermal ablation. A new type of HIFU therapy—boiling histotripsy (BH)—aims at mechanical fractionation of into subcellular fragments, with a range of accompanying thermal effects that can be tuned from none to substantial depending on the requirements of the application. The degree of mechanical tissue damage induced by BH has been shown to depend on the tissue type, with collagenous structures being most resistant, and cellular structures being most sensitive. This has been reported for single BH lesions, but has not been replicated in large volumes. Such tissue selectivity effect has potential uses involving tissue decellularization for biofabrication technologies as well as mechanical ablation by BH while sparing critical structures. The goal of this study was to investigate tissue decellularization effect in larger, clinically relevant liquefied volumes of tissue, and to evaluate the accumulated thermal effect in the volumetric lesions under different exposure parameters. All BH exposures were performed with a 256-element 1.2 MHz array of a magnetic resonance imaging—guided HIFU (MR-HIFU) clinical system (Sonalleve V1, Profound Medical Inc, Mississauga, Canada). The volumetric BH lesions were produced in degassed *ex vivo* bovine liver using 1–10 ms long pulses with *in situ* shock amplitudes of 75–100 MPa at the focus and pulse repetition frequencies (PRFs) of 1–10 Hz covering a range of effects from pure mechanical homogenization to thermal ablation. Multimodal analysis of the lesions was then performed, including microstructure (histological), ultrastructure (electron microscopy), and molecular (biochemistry) methods. Results show a range of tissue effects in terms of the degree of tissue selectivity and the amount of heat generated in large BH lesions, thereby demonstrating potential for treatments tailored to different clinical applications.

1. Introduction

New types of high intensity focused ultrasound (HIFU) therapy resulting in mechanical homogenization of tissue, namely, cavitation-based histotripsy and boiling histotripsy (BH) have shown great promise for clinical use (Maxwell *et al* 2012, Hoogenboom *et al* 2015, Khokhlova *et al* 2015). BH uses milliseconds-long bursts of nonlinear HIFU waves containing shocks that develop at the focus to repeatedly induce boiling at the focus within

each burst; the interaction of the remaining part of the incident HIFU burst with a vapor bubble homogenizes tissue through the mechanism of acoustic atomization (Khokhlova *et al* 2011, Simon *et al* 2012). The degree of mechanical tissue damage induced by both types of histotripsy depends on the tissue type. In general, the more fibrous structures such as vasculature are able to resist mechanical disruption while cells are more easily lysed (Vlaisavljevich *et al* 2014). This effect has been demonstrated by a number of groups in a number of tissues, both *ex vivo* (Lake *et al* 2008b, Vlaisavljevich *et al* 2014, Khokhlova *et al* 2015, Eranki *et al* 2017) and *in vivo* (Lake *et al* 2008a, Schade *et al* 2012). This attribute holds clinical promise as many HIFU applications require the sparing of critical tissue structures, such as vessels and ducts adjacent to, or within, the treatment site. This tissue selectivity effect also has potential uses for developing biocompatible scaffolds and noninvasively decellularizing tissue in regenerative medicine (Pahk *et al* 2016, Khokhlova *et al* 2017a). Sparing of small segments of biliary structures and vessels was previously demonstrated *in vivo* for single BH lesions in porcine liver (Khokhlova *et al* 2014). However, the specifics of the size range of preserved connective tissue structures, potential alterations to the smallest structures, and the dependence thereof on BH exposure parameters were not investigated in that work. One way to perform this investigation is to produce volumetric BH lesions that contain a large region of the connective tissue network to include a range of structural sizes. Further, it was also previously shown for single BH lesions, both *ex vivo* and *in vivo*, that the amount of thermal effect can be controlled by the choice of BH exposure parameters and can range from virtually none to substantial (Wang *et al* 2013, Khokhlova *et al* 2014). In certain clinical scenarios it may be beneficial to have a thermal component to the treatment, and the specific pulsing parameters (primarily duty cycle and pulse duration) may differ in the degree of thermal effect induced in single versus volumetric lesions due to heat diffusion and fluid convection within the lesion. However, there could also be complications related to thermal damage to nerves and blood vessels. Thus, the primary goal of this work was to evaluate the residual connective tissue structure network and the extent of thermal effect in volumetric BH lesions produced by different pulsing protocols in *ex vivo* liver tissue using a clinical HIFU transducer array.

2. Materials and methods

2.1. Experimental arrangement

A clinical 3.0T magnetic resonance imaging—guided HIFU (MR-HIFU) system (Sonalleve V1, Profound Medical Inc, Mississauga, Canada) installed at the Bio-Molecular Imaging Center at the University of Washington (Seattle, WA) was used to apply the BH regimens. The system included a 1.2 MHz, 256-element transducer array attached to a positioning system with 5 degrees of freedom inside a patient table. The transducer was housed in oil and comprised 256 circular elements with 6.6 mm diameters, with an overall aperture of 127.8 mm and a nominal focal length of 120 mm, with the full width and length (i.e. between the nulls of the pressure field) of the focal lobe were 2.5 mm and 15 mm, correspondingly (Kreider *et al* 2013). For these experiments, most sonications were performed with the patient table outside the room with the 3.0T MRI unit, and some sonications aimed at measuring the temperature inside BH lesions during treatment were performed inside the magnet bore. A cylindrical acrylic tank (inner diameter of 184 mm) was attached to the top of the patient table and filled with degassed phosphate buffered saline. This arrangement is depicted in figure 1, which illustrates that the ultrasound beam propagates through oil and a Mylar membrane before entering the tank in which target tissue samples were held.

2.2. Sonication procedure

Bovine liver from freshly slaughtered animals was obtained from a local abattoir, placed on ice and used in the experiment within 8 h. Prior to BH exposures, the liver was cut into cuboid samples of $5 \times 5 \times 5$ cm size, placed into degassed cold phosphate buffered saline and degassed in a desiccant chamber for at least 1 h. The samples were then transferred into a custom-built plastic holder and placed into the cylindrical tank such that the geometrical focus of the HIFU array was 20 mm deep in the tissue.

During BH sonications to create volumetric lesions, the HIFU focus was electronically steered in directions along the beam axis and transverse to it. For a given axial depth, sonication trajectories within the transverse plane comprised concentric rings, with a radial spacing of 2 mm between target sites in each ring (see inset in figure 1). The maximum applied steering range in the transverse direction was 8 mm. Overall volumes included sonications in layers at two or three depths, with 5 mm between layers. The spacing between the lesions in both axial and transverse directions was determined in preliminary experiments such that the individual lesions would fully merge. An example photograph of an individual BH lesion is shown in an inset to figure 1. It was confirmed that the lesion shape and size did not depend on the focus steering location up to 8 mm off axis. Within a given layer, a single BH pulse was delivered to each site of the trajectory by raster-scanning the focus location in sequence, and the entire sequence was repeated until each point received a total of 30 BH pulses. Within each concentric ring, consecutive BH pulses were delivered to sites that were furthest apart to minimize heat build-up. The progression

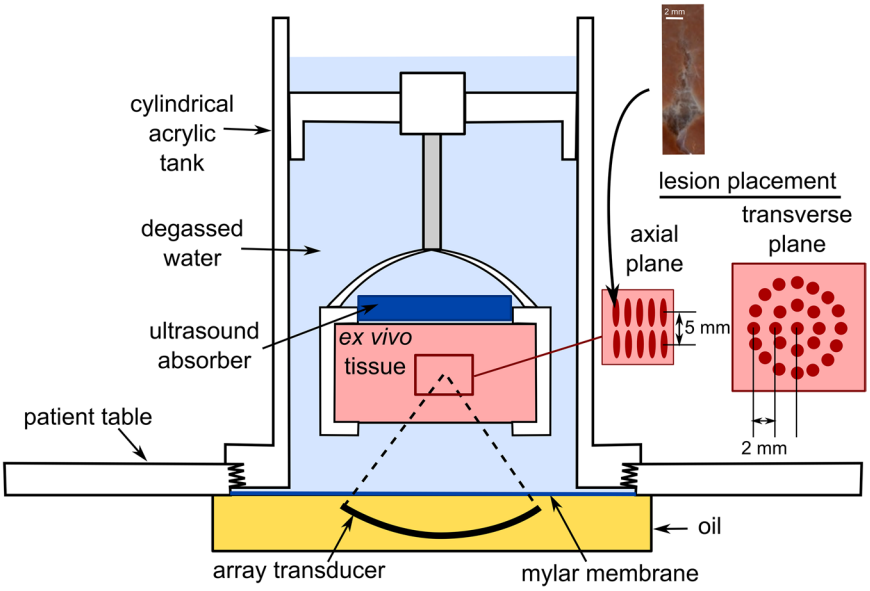

Figure 1. Experimental setup for producing volumetric BH lesions in *ex vivo* bovine liver samples using Sonalleve V1 array transducer. Smaller volumetric lesions were produced by electronically steering the HIFU focus onto individual sites arranged as a central site and two concentric circles in two depth layers (see the insert on the right). A single BH pulse was delivered at each site within a layer, and then the sonication along the trajectory was repeated until each site received a total of 30 BH pulses. Spacing between trajectory sites was chosen such that the individual cavities (see example photo on top) would merge. The steering trajectory within each circle was arranged such that consecutive BH pulses were delivered to the sites furthest away from each other to minimize heat accumulation. Larger lesions were produced with four concentric circles and three depth layers.

between layers was performed by electronically shifting the transducer focus in the axial direction toward the transducer by 5 mm. The Lesions with two transverse sizes were produced: 1 cm (transverse steering up to 4 mm, 25 sonication points per layer) and 2 cm (transverse steering up to 8 mm, 81 sonication points per layer). In each tissue sample, either four volumetric lesions of 1 cm diameter or one lesion of 2 cm diameter were produced. At least eight volumetric lesions were produced for each exposure parameter: Five to six lesions of each kind was bisected, analyzed grossly, with content sampled for protein analysis and ultrastructural evaluation. One set of lesions were frozen embedded *en bloc*. Another set of lesions was fixed in 10% neutral buffered formalin *en bloc* and used for histological evaluation.

2.3. Exposure parameters

The BH exposure parameters and the geometric parameters of the beam steering trajectories are summarized in table 1. Two combinations of acoustic power and pulse duration were used in the study to evaluate the effect of the shock amplitude and pulse duration on the treatment outcome: 10 ms long pulses at 250 W acoustic power and 1 ms long pulses at 600 W acoustic power. Initiation of boiling within each pulse was assumed for both power settings; as demonstrated in our prior studies, under this condition the size and shape of an individual BH lesion was expected to be the same for both cases, therefore the spacing between the focal sites was kept constant (Khokhlova *et al* 2017b). To predict the time to reach boiling temperature at the focus in *ex vivo* liver tissue at each of the acoustic power settings, the weak shock theory was used (Hamilton and Blackstock 1998, Canney *et al* 2010):

$$t_b = \frac{\Delta T}{C}\frac{6\rho c^4}{\beta f_0 A_S^3}, \tag{1}$$

where ΔT is the change from the measured ambient water temperature in the tank of 22 °C to 100 °C, f_0 is the fundamental ultrasound frequency, A_S is the shock amplitude in the focal waveform *in situ*; acoustic and thermal properties of liver tissue were estimated from the literature as: $C = 3060{\cdot}10^3$ J/m^3/°C—the specific heat, $\beta = 4.8$—the coefficient of nonlinearity, $\rho = 1050$ kg m^{-3}—the density, and $c = 1580$ m s^{-1}—the sound speed in tissue (Duck 1990). To obtain the *in situ* shock amplitudes and peak focal pressures, the focal waveforms measured in water in our previous study (Kreider *et al* 2013) were derated into 2 cm depth in liver tissue. To account for ultrasound attenuation in tissue (assumed as 0.065 Np cm^{-1}), modified nonlinear derating approach was used (Bessonova *et al* 2010).

At the acoustic power of 250 W the predicted time to reach boiling at the focus was 6.3 ms—shorter than the pulse duration (10 ms), such that boiling was initiated by each pulse. The use of the higher acoustic power setting

Table 1. HIFU treatment parameters.

	Small lesions	Large lesions
Lesion diameter	1 cm	2 cm
Number of layers	Two layers	Three layers
Acoustic power	250 W	600 W
Pulse length	10 ms	1 ms
Duty cycle	1, 3, 5, 10%	0.4%
In situ p^+/p^-	+75/−10.5 MPa	+92/−15.7 MPa

of 600 W corresponded to shorter predicted time to boiling (1.3 ms). Although that time was slightly longer than the pulse duration (1 ms), our previous experimental observations showed that at these conditions liquefied BH lesions still successfully formed (Khokhlova *et al* 2017b). One possible explanation is the formation of a large bubble at the HIFU focus at the temperatures slightly below 100 °C. As previously reported by Vlaisavljevich *et al* (2016), the intrinsic threshold for cavitation in water is reduced at elevated temperatures from 28.9 MPa at 20 °C to 17.4 MPa at 80 °C and 14.9 MPa at 90 °C. In our case, peak negative focal pressure was 15.7 MPa, and the temperatures within 80 °C–90 °C could be reached within 1 ms. Therefore, this pulsing regime may represent a merge between BH and microtripsy mechanisms.

The influence of duty cycle on the treatment outcome was evaluated at the lower acoustic power level of 250 W by keeping pulse duration the same (10 ms) and increasing pulse repetition frequency over the range of 1–10 Hz which corresponded to the 1%–10% duty cycle. Duty cycle of 0.4% was used for high power exposures to minimize thermal effects.

2.4. MR thermometry

A limited set of sonications in each of the pulsing regimes was performed inside the bore of the 3.0T magnet to measure intra- and post-sonication temperature changes using a dynamic, multishot, RF-spoiled, fast-field-echo (FFE)—based pulse sequence and the proton resonance frequency shift (PRFS) thermometry—method (Ishihara 1995). To cover the whole target region, five imaging slices were acquired perpendicular to the beam axis and one slice was acquired parallel to the beam axis. The imaging parameters were: TR 39 ms, TE 16 ms, matrix 224 × 224, FOV 400 × 400 mm^2, slice thickness 5 mm, and flip angle 19°, resulting in spatial acquisition resolution of 1.8 mm × 1.8 mm × 5.0 mm, with an acquisition time of 7.5 s per dynamic frame. MRI-based temperature data was analyzed from the centermost imaging slice acquired perpendicular to the beam axis in 5 × 5 voxel and 11 × 11 voxel rectangular regions-of-interest (ROI) for 1 cm and 2 cm-diameter lesions, respectively, and centered on the lesion. The baseline tissue temperature was set to 23 °C.

2.5. Histology

After treatment, the lesions were either fixed in 10% neutral buffered formalin *en bloc* or embedded in optimum cutting temperature medium by submersion in isopentane cooled on dry ice. The 5 μm sections were taken and stained with Hematoxylin and Eosin (H&E) or Masson's trichrome for the fixed tissue. Frozen sections (8 μm) were stained with NADH-diaphorase (Wang *et al* 2013) to evaluate thermal denaturation.

2.6. Protein analysis

To quantitatively compare the extent of thermal denaturation of the lesion contents produced at lower acoustic power of 250 W and increasing duty cycle of 1, 3, 5 and 10%, protein analysis was performed according to the following protocol. The very top of the tissue was removed while maintaining the sample in a vertical position to gain access to the lesion contents. For the liquid and paste lesions, a small pipette was used to remove the sample contents. For solid lesions, the center of the lesion was removed and finely minced using two razor blades. The samples from all lesions were subject to a series of water and salt extractions as described previously (Wang *et al* 2013). The pooled extractions were evaluated by a colorimetric assay (Coomassie Plus Bradford Protein Assay). A standard protein curve was used to determine the concentration in solution. The concentrations were normalized by the wet weight of the sample to give a number of milligram protein per milligram of tissue. Small parts of untreated tissue samples were taken for baseline control measurements. The concentration of denatured protein in each sample was presented as the percent of denatured protein relative to the mean protein in the baseline control samples.

2.7. Electron microscopy

Samples were also taken for transmission electron microscopy (TEM) from lesions sampled for protein analysis. Once the samples were taken, they were immediately embedded in HistoGel™ (Thermo Scientific, Waltham, MA) using standard protocols. The HistoGel containing the lesion contents were cut into small blocks (1 × 1 × 5 mm)

and submerged in ½ strength Karnovsky's fixative before being processed for TEM. Briefly, the fixed samples were stained with 1% OsO4 in phosphate buffered saline (PBS), before being dehydrated in ascending acetone concentrations and embedded in EPON-Araldite mixture resin. After polymerization, 80 nm thick sections were cut on an LKB ultramicrotome. Sections were collected on carbon coated Cu grids and stained with lead citrate according to Reynolds (1963). Grids were visualized using a transmission electron microscope JEOL JEM-1011 (Jeol USA Inc, Peapody, MA, USA), and representative images were taken at 80 kV using a GATAN SC1000W camera with 8.5 Mpixels resolution (Gatan Inc, Pleasonton, CA, USA) and Micrograph software.

2.8. Statistics

Comparisons between groups were performed using a one-way independent ANOVA using StatPlus (AnalystSoft, Walnut, CA, USA). Differences were considered statistically significant after Bonferroni correction ($p < 0.0125$).

3. Results

3.1. Gross evaluation and histology

The figures presented in this section are typical examples of the lesions produced using the BH-HIFU regimens applied. Photographs of the cross-sections of the lesions produced at lower acoustic power of 250 W and 10 ms pulses with increasing duty cycle are presented side by side with those with the liquid/paste contents washed out (figure 2). The lesion contents could be washed out easily without agitation in the lesions formed with duty cycles of 1% and 3%, revealing remaining connective tissue not homogenized by the treatment. This remaining tissue was pliable and easily manipulated (figure 3). With increasing duty cycle, the lesion contents became whiter and more viscous, representing 'paste' content in agreement with our observations of single BH lesions (Wang *et al* 2013). In the 5% and 10% duty cycle lesions, there was some remaining connective tissue that was not homogenized by the treatment, but this tissue was increasingly more friable with increase in duty cycle. An outer white ring caused by diffusion of heat could be observed in the lesions formed with 3%, 5% and 10% duty cycles, with increasing severity. The extent of tissue blanching around the lesion was approximately 250 μm, 800 μm, and 3 mm at 3, 5, and 10% duty cycle respectively. NADH-diaphorase staining (figure 2) indicates partial thermal denaturation in the 3% duty cycle lesion and complete thermal denaturation in the 5% and 10% duty cycle lesions with surrounding borders matching the denaturated white rings observed with gross evaluation (figure 2). These findings correspond well to the MR thermometry data. Specifically, for the lesions sonicated at 250 W and 1%, 3%, 5%, and 10% duty factors, the peak mean MRI-measured temperatures within the ROIs (i.e. within the volumetric lesions), were 38.2 °C ± 0.8 °C, 58.1 °C ± 1.1 °C, 68.9 °C ± 1.8 °C, and 99.6 °C ± 4.0 °C, respectively. For the lesion sonicated at 600 W and 0.4% duty cycle the peak mean temperature was 40.0 °C ± 0.7 °C.

Histological evaluation of the lesions at higher magnification (figure 4) showed that at 1% duty cycle cellular tissue was completely homogenized (figure 4). Some nuclear fragments were observed within the lesion. With increasing duty cycle, the number of nuclear fragments increased, and the contents of the lesion became more textured indicating thermal coagulation. At 1% duty cycle, some vacuoles were observed at the border (approximately 100 μm thick) of the corresponding lesion. The vacuoles were also observed in some of the lesions formed at 3% duty cycle but were less apparent than these formed at 1% duty cycle. The vacuoles were not observed in the 5% and 10% duty cycle lesions. Instead, heat fixed tissue that was more eosinophilic was present at the border of these lesions which matched the blanching observed grossly. This increase in eosinophilic intensity was likely due to tissue dehydration and was thus an indirect indication of the thermal coagulation of tissue. Masson's trichrome stained sections revealed intact fibrillar collagen in the lesions treated at 1% and 3% duty cycles. Within and close to the fibrillar collagen, intact vessels and ducts could be observed. At the 1% duty cycle, small caliber ($<$30 μm) vessels and bile ducts were observed within the collagen. With increasing duty cycle, the collagen became more globular and fewer small caliber vessels and ducts could be observed.

Histological evaluation of the lesions at higher magnification (figure 4) showed that at 1% duty cycle cellular tissue was completely homogenized (figure 4). Some nuclear fragments were observed within the lesion. With increasing duty cycle, the number of nuclear fragments increased,and the contents of the lesion became more textured indicating thermal coagulation. At 1% duty cycle, some vacuoles were observed at the border (approximately 100 μm thick) of the corresponding lesion. The vacuoles were also observed in some of the lesions formed at 3% duty cycle but were less apparent than these formed at 1% duty cycle. The vacuoles were not observed in the 5% and 10% duty cycle lesions. Instead, heat fixed tissue that was more eosinophilic was present at the border of these lesions which matched the blanching observed grossly. This increase in eosinophilic intensity was likely due to tissue dehydration and was thus an indirect indication of the thermal coagulation of tissue. Masson's trichrome stained sections revealed intact fibrillar collagen in the lesions treated at 1% and 3% duty cycles. Within and close to the fibrillar collagen, intact vessels and ducts could be observed. At the 1% duty cycle, small caliber

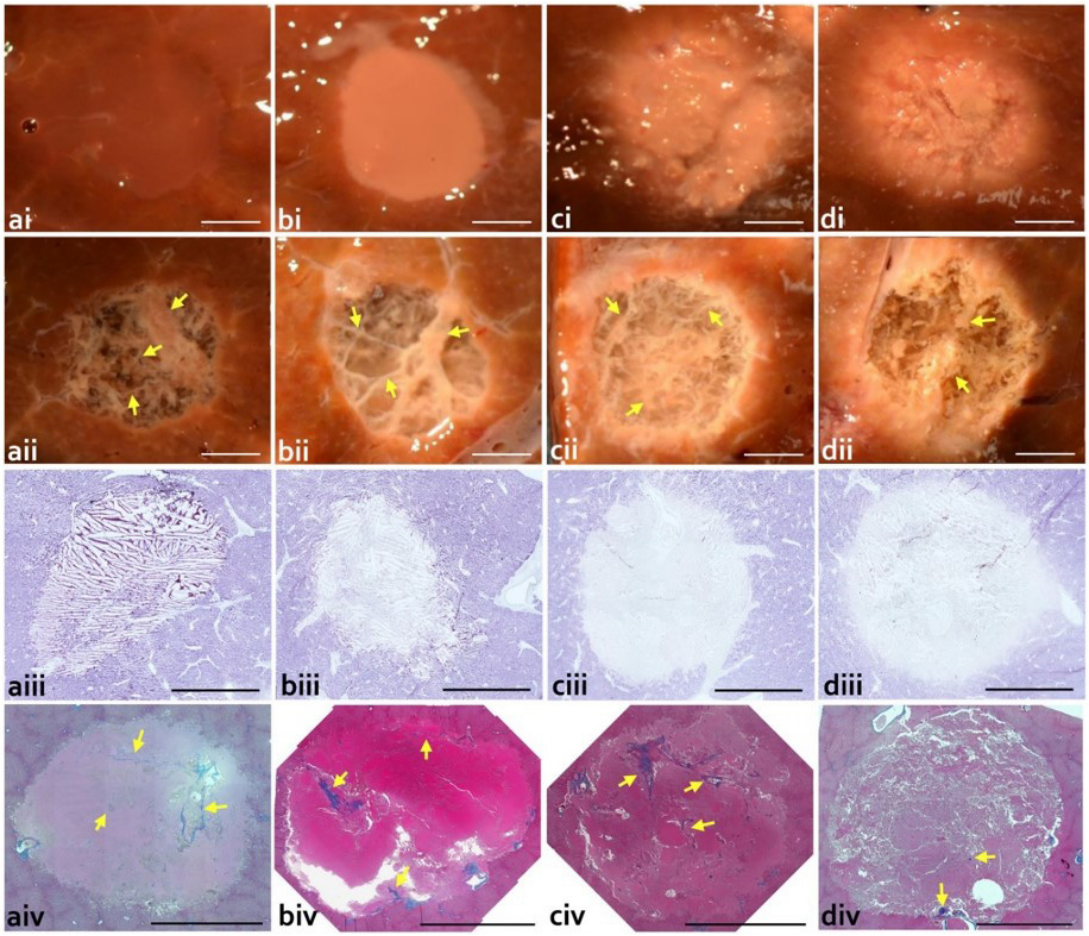

Figure 2. Gross and histological evaluation of the volumetric lesions produced at the lower acoustic output power of 250 W, with pulse duration of 10 ms and varying duty cycle: (a) 1%; (b) 3%; (c) 5%; (d) 10%. Upper rows show photos of lesions in cross-section (i) before and (ii) after rinsing the contents out. Rinsed lesions reveal connective tissue (yellow arrow) that was not liquefied by the treatment. Higher duty cycle lesions show a blanched border surrounding the lesion. NADH-diaphorase stained sections (iii) reveal minimal thermal denaturation at (a) 1% duty cycle; some thermal denaturation at (b) 3% duty cycle; and almost complete thermal denaturation at the (c) 5% and (d) 10% duty cycles. Massons trichrome stained histological sections (iv) confirm the presence of connective tissue appearing in the native state within the lesions (yellow arrow). Scale bar represents 5 mm.

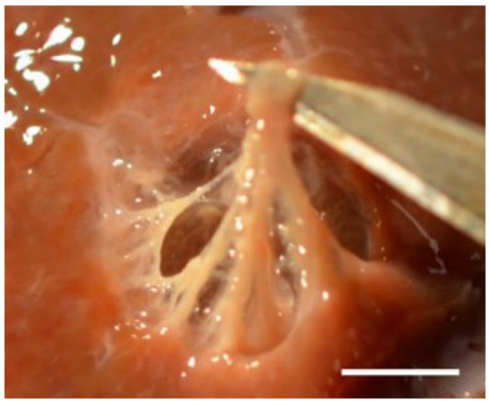

Figure 3. Photograph of the volumetric lesion (250 W, 10 ms pulses, 3% duty cycle) with lysed cell debris washed out and with the remaining connective tissue manipulated showing the pliability of the remaining connective tissue. Scale bar represents 5 mm.

(<30 μm) vessels and bile ducts were observed within the collagen. With increasing duty cycle, the collagen became more globular and fewer small caliber vessels and ducts could be observed.

The gross appearance of the lesion produced at higher acoustic power of 600 W, with shorter 1 ms BH pulses and 0.4% duty cycle (figure 5), was similar to that of the lesions formed at lower power with 10 ms pulses at 1% duty cycle (figures 2(a) and (b)). With the homogenized contents washed out, a fine structure of remaining connective tissue was observed throughout the lesion. Histological evaluation of the rinsed lesion revealed connec-

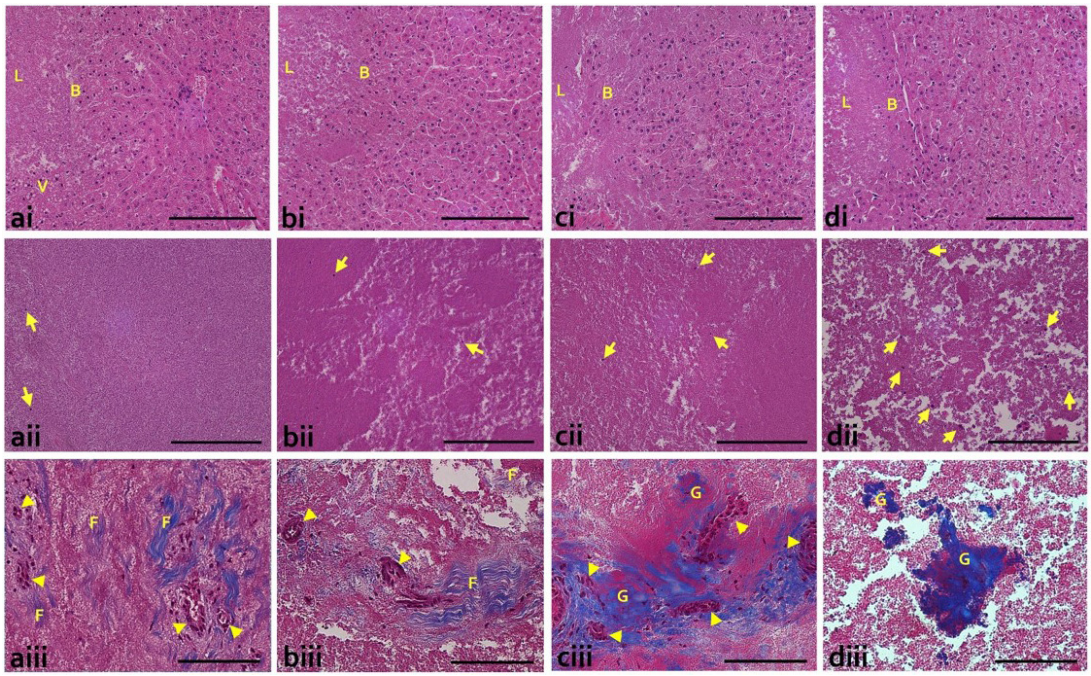

Figure 4. Histomicrographs of representative lesion sections from figure 2 stained with Hematoxylin and Eosin and showing the (i) lesion (L) and lesion border (B) and (ii) central portion of the lesions treated at (a) 1%; (b) 3%; (c) 5%; and d) 10% duty cycle. In the border of the (a) 1% duty cycle lesion, there were some vacuoles (V) present which was not observed for the 3, 5 or 10% duty cycles. The (a) 1% duty cycle resulted in a uniformly homogenized tissue with some nuclear fragments (yellow arrow). With increasing duty cycle, the number of nuclear fragments (yellow arrow) increased and the contents of the lesion became more textured indicating thermal coagulation. Scale bar represents 200 μm. (iii) High magnification of Masson's trichrome stained sections reveal intact fibrillar collagen (F) present in lesions treated with (a) 1% duty cycle and (b) 3% duty cycle. With the higher duty cycles, the collagen becomes globular (G), with the (d) 10% duty cycle having a greater amount of globular collagen than the (c) 5% duty cycle. Close to the collagen, small caliber vessels and ducts (yellow arrow head) were present in many of the lesions. Scale bar represents 100 μm.

tive tissue extended throughout the depth of the lesion (figure 5). A greater number of small caliber (<20 μm) vessels and ducts were observed to be patent and surrounded by fibrillar extracellular matrix. In addition, finer connective tissue structures were present within this lesion.

The time to produce the smaller lesions of 1.2 × 1 cm size varied within 25–2.5 min range, depending on the duty factor (and hence the PRF) employed, resulting in the ablation rate of 2.4–24 cc h^{-1}, correspondingly. Generation of the lesion at higher acoustic power and increased PRF (larger lesion, 2 cm × 1.5 cm) took 30 min, corresponding to the ablation rate of 10 cc h^{-1}.

3.2. Protein analysis

There was increasing amounts of thermal damage to the tissue with increasing duty cycle, as evident in the amount of insoluble protein, which can be a measure of thermal denaturation (figure 6). There was almost complete denaturation within the 10% duty cycle lesion. The amount of denatured protein was significantly less for the 1% and 3% lesions compared to either the 5% or 10% duty cycle lesions.

3.3. Electron microscopy

Figure 7 shows the representative TEM images. Untreated tissue showed a generally normal appearance with an intact nucleus with disperse chromatin. However, a mild general edema was present as evident by slightly swollen mitochondria with some loss of membrane cristae (figure 7(a)). In all treated lesions, all cellular structure was lost (figures 7(b)–(e)). The cytoplasmic cell membranes were absent and cellular components were not distinguishable. Ghosts of organelles could be observed in the form of membranous structures of variable size and electron density amongst a sea of cellular debris. With increasing duty factor there was evidence of a gradient increase in thermal application. The cellular debris became more condensed and as such, more electron dense with increasing duty factor, consistent with heat coagulation of proteins. Non-coagulated proteins were observed in a higher percent at the lower duty factors.

4. Discussion

In this work, a clinical MR-HIFU system was used to perform volumetric BH ablation of *ex vivo* bovine liver tissue and to investigate the effects of pulsing parameters on the treatment outcome. As the BH technology

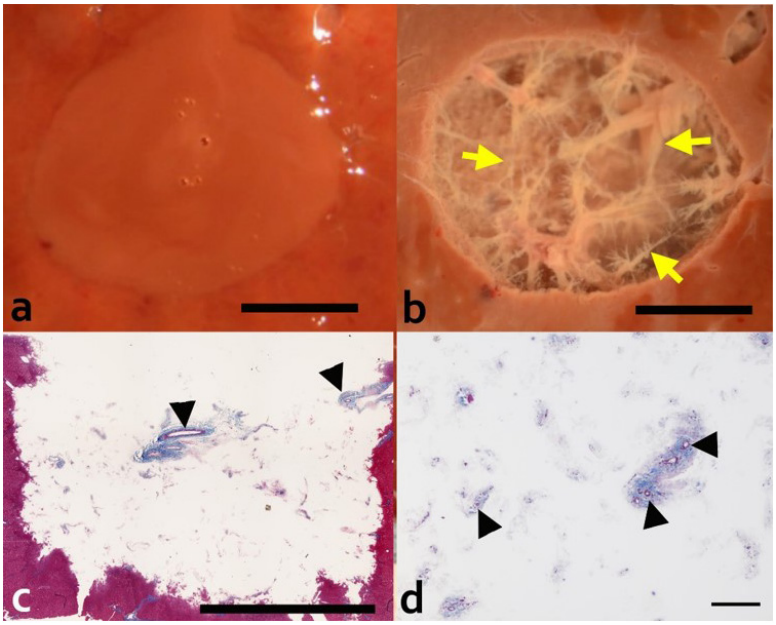

Figure 5. Gross and histological evaluation of the 2 cm diameter volumetric lesion generated with 1 ms pulses at 600 W peak acoustic power and 0.4% dc. Upper row show photos of lesions in cross-section (a) before and (b) after rinsing the contents out. Rinsed lesions reveal connective tissue (yellow arrow) that was not liquefied by the treatment. Masson's trichrome stained histological sections of the rinsed lesion (longitudinal orientation) (c) confirm the presence of connective tissue appearing in the native state throughout the depth of the lesion. Scale bar represents 1 cm. (d) Higher magnification of the lesion with the homogenized contents washed out reveals intact fibrillar collagen with patent small caliber vessels and ducts (black arrow head). Scale bar represents 250 μm.

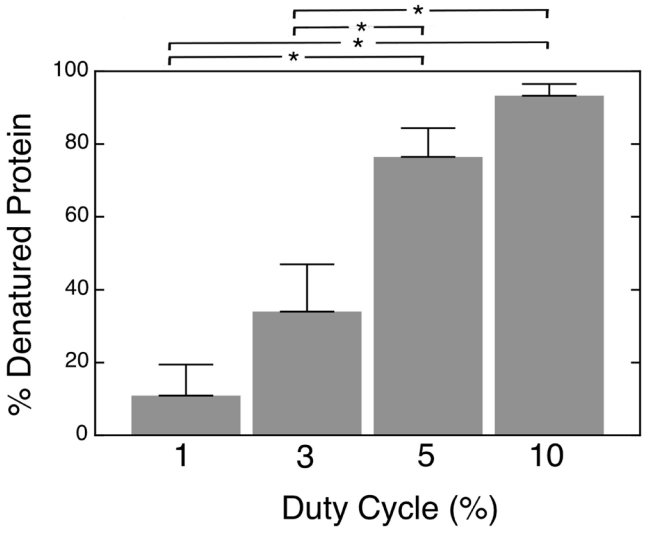

Figure 6. Percent of denatured water-and-salt-insoluble proteins extracted from the volumetric lesions generated at 250 W acoustic power with 10 ms-long pulses and varying duty cycle, relative to control tissue. Percent of insoluble protein was used as a quantitative measure of the thermal effect as solubility is lost with thermal denaturation. Error bars represent standard deviation, $n = 5$–6. * indicates statistically significant differences ($p < 0.0125$).

progresses toward clinical translation, the understanding of ways to control the treatment outcome is paramount. Specifically, the extent of thermal denaturation within and around the lesion, cellular homogenization, and extracellular matrix sparing were examined using gross, histological, ultrastructural, and biochemical methods. Previous studies have shown that in single BH lesions these effects can be controlled both *ex vivo* and *in vivo* through the choice of pulsing parameters (Wang *et al* 2013, Khokhlova *et al* 2014). Here, the applicability of those findings to clinically relevant large volumetric lesions was evaluated.

At all pulsing protocols examined, the cells within volumetric lesions were fully homogenized, whereas varying amounts of intact extracellular matrix remained, which is consistent with previously reported evaluation of single BH lesions, as well as cavitation-based histotripsy lesions (Vlaisavljevich *et al* 2013, Wang *et al* 2013, Khokhlova *et al* 2014). The gross images, histological, ultrastructural, and biochemical analysis supported

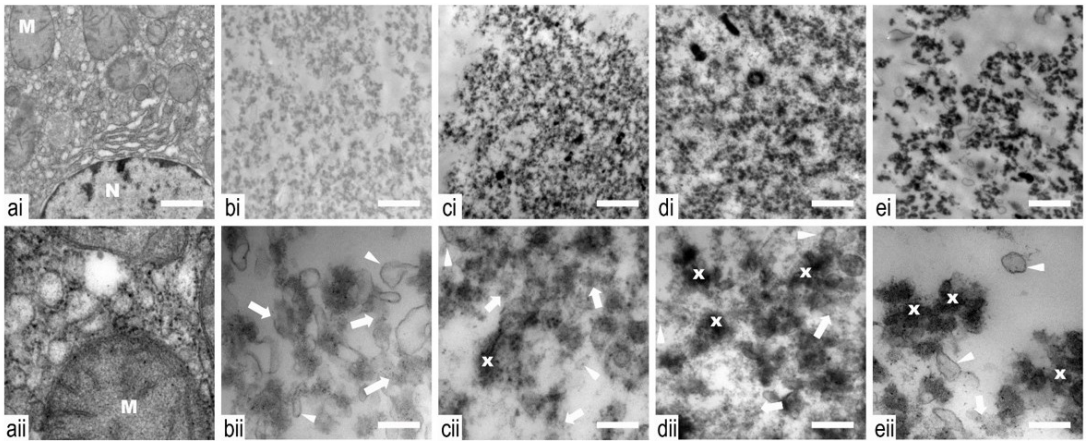

Figure 7. Transmission electron microscopy images of samples taken from control (a) and histotripsy lesions produced with a range of duty cycles: 1 (b), 3 (c), 5 (d) and 10% (e), obtained at low (i) and high (ii) magnifications. Untreated tissue (a) shows a generally normal appearance with an intact nucleus (N) with disperse chromatin. A mild general edema is present as evident by slightly swollen mitochondria (M) with some loss of membrane cristae, which can be expected in *ex vivo* tissue. With treatment, and at all duty cycles, all cellular structure is lost. The cytoplasmic cell membranes are absent and cellular components are not distinguishable. Ghosts of organelles can be observed in the form of membranous structures (white arrow head) of variable size and electron density amongst a sea of cellular debris. With increasing duty cycle, there is evidence of a gradient increase in thermal application. The cellular debris become more condensed (x) and electron dense with increasing duty factor, consistent with heat coagulation of proteins. Non coagulated proteins are observed in a higher percent at the lower duty factors (white arrow). Low (i) and high (ii) magnification scale bar represents 1 μm and 250 nm, respectively.

the observation that the increase of duty cycle (3% and higher) resulted in a gradually increasing amount of thermally denatured proteins within the lesion, an increase in viscosity of the lesion contents in addition to thermal effects observed in the remaining extracellular matrix. This observation is also in agreement with our previous investigations of single BH lesions (Khokhlova *et al* 2011, Wang *et al* 2013): in order to avoid the accumulation of heat over the course of BH exposure and the associated tissue effects, the duty factor should be less than 3%. Theoretically, heat accumulation during the generation of volumetric BH lesions was expected to be larger compared to single lesions because the rate of heat diffusion out of the lesion is lower for a larger volume, whereas the rate of heat deposition per unit volume is the same. However, likely due to the choice of sonication trajectory, where the consecutive foci within the rings were placed as far apart as possible, heat build-up was minimized, and appeared to be the same as that for single BH lesions.

Other important factors to consider when applying the results of this study to *in vivo* sonications are the absence of perfusion in *ex vivo* tissue samples used in this work and the starting tissue temperature being lower (23 °C versus 37 °C) than *in vivo*. These two factors should have opposite effects on BH-induced heat accumulation in tissue and degree of thermal denaturation. In our prior experience with single BH lesions in porcine liver, the thermal effects were found only slightly more pronounced *in vivo* than *ex vivo* given the same BH exposure conditions (Khokhlova *et al* 2014). However, the exact extent of heat sinking or heat accumulation is expected to be highly tissue and organ-dependent and can only be evaluated *in vivo*.

Important practical aspects with regards to the capabilities of the clinical system in performing BH are the maximum depth in tissue at which the treatment would be feasible given the power output limitations of the system, as well as the achievable ablation rate. In research mode, the maximum output acoustic power achievable with V1 system is 1200 Watts. Assuming average attenuation in soft tissues of 0.75 dB cm^{-1} at 1.2 MHz, and the output power levels of 250 W and 600 W for long and short BH pulses, correspondingly, that was sufficient for treatment at the depth of 2 cm, the maximum achievable depths would be 11 cm and 6 cm, correspondingly. In terms of ablation rate, the treatment delivered at higher duty factor and resulting in higher degree of thermal denaturation was also faster compared to the treatment resulting in purely mechanical fractionation due to the higher PRF used, given the fixed number of pulses delivered per focal site. There are at least two ways that we have previously demonstrated to result in acceleration of mechanical fractionation rate, one of which was partially tested in this work. Specifically, the use of shorter, but higher amplitude BH pulses delivered at higher PRF, such that the duty factor remains constant, results in treatment acceleration that is proportional to PRF. This is because the size of a single BH lesion depends on the number of pulses applied rather than the total 'HIFU on' time (Khokhlova *et al* 2017b). Therefore, in this work the use of PRF of 4 Hz with the shorter 1 ms pulses resulted in a 4-fold increase in ablation rate compared to the PRF of 1 Hz. This ablation rate could be further increased by using the PRF of up to 10 Hz, resulting in the duty cycle of 1% and ablation rate of 24 cc h^{-1}. The second way to enhance mechanical ablation rate is to use tighter spacing of the focal sites (e.g. 1 mm as opposed to 2 mm used

here) and delivering fewer BH pulses per focal site (e.g. 2–5 pulses versus 30 pulses used here). This is because the dependence of the lesion size on the number of delivered pulses has a saturating behavior (Khokhlova *et al* 2016).

In this study, the ultrastructural evaluation of the liquid contents of the BH lesion was performed for the first time. Complete loss of the cellular structure was confirmed in all treated samples: all cellular membranes were absent, only occasional ghosts of organelles were observed in some samples. With increasing thermal effect, cellular debris were observed to become more condensed, consistent with heat coagulation of protein. The complete destruction of cells could alleviate the threat of releasing viable tumor cells into the circulation and the risk of metastasis (Styn *et al* 2010). In addition, it is possible that the availability of non-denatured tumor-associated antigens could instead elicit an immune response resulting in an anti-tumor effect (Hu *et al* 2007, Khokhlova *et al* 2015). The limitation of this part of the study is that ultrastructural evaluation was only performed with the liquefied debris, but not the extracellular matrix and connective structures that were left behind. This will be performed in future studies.

With regards to the treatment effect on connective tissue structures, lower duty cycles, as well as shorter BH pulses were observed to result in finer structures left intact. Specifically, at a duty cycle of 10%, it was difficult to distinguish if the smaller caliber vessels were intact due to overall disruption of tissue. It is possible that the accumulation of heat and thermal effect on collagen fibers made the small caliber vessels more susceptible to mechanical insult. This speculation is in qualitative agreement with observations presented in Vlaisavljevich *et al* (2015), where susceptibility of different tissues to cavitation-based histotripsy was investigated after thermal pre-conditioning at 60 °C or 90 °C. It was shown that after heating of the tissue for several hours up to 60 °C the tissues became less stiff and more susceptible to cavitation-based damage, whereas heating to 90 °C made them stiffer. In present experiments, the overall sonication duration was less than 30 min, and the MR-measured peak mean temperatures were over 60 °C for 5% duty cycle and over 90 °C for the 10% duty cycle. With lower duty cycles, peak mean MR-measured temperatures were lower than 60 °C, and small vessels were observed macroscopically and histologically, and the preserved structure was pliable upon manipulation. Finer sized vessels were present in a lesion obtained with high amplitude 1 ms pulses as compared to smaller amplitude 10 ms pulses. These vessels and ducts appeared to be patent, which could be important in both tumor treatment and for tissue engineering application. If this treatment is used to debulk tumor tissue, the remaining patent vessels could allow the delivery of drugs to the region. In tissue engineering, viable vessels could be used for delivering nutrients to cells injected to replace the diseased tissue (Pahk *et al* 2016); or could serve as biomimetic scaffolds ready for recellularization with autologous cells *in vivo* (Khokhlova *et al* 2017a). However, further evaluation either *in vivo* or in artificially perfused organ, is needed to determine if there is any damage to the vessels and ducts to render them non-functional. In this study, although some damage to collagen was observed in all lesions, the extent of the damage was not evaluated. It is likely that the treatment parameters could be further optimized to result in complete decellularization with minimal connective tissue damage, whilst preserving essential extracellular matrix elements. Future studies will include detailed quantitative analysis of the structure of the BH lesions generated using a clinical MR-guided system.

5. Conclusions

This study demonstrates that BH mechanical ablation can be performed by a clinical HIFU system for volumetric decellularization of liver tissue with the ability to control the amount of thermal effect and to preserve certain 3D tissue structures like vessels and ducts. With further tailoring of the pulsing scheme parameters, this treatment modality could potentially be utilized for multiple applications where selective disruption of tissue is desirable, such as in tumor ablation and decellularization of organs for tissue engineering applications.

Acknowledgments

This work was supported by NIH EB007643, K01 EB 015745, NIH R21CA219793 and RFBR 16-02-00653 and RFBR 17-54-33034 grants. The authors thank the Electron Microscopy Laboratory of the Biological Faculty of Moscow State University for the help in TEM analysis.

References

Bessonova O V, Khokhlova V A, Canney M S, Bailey M R and Crum L A 2010 A derating method for therapeutic applications of high intensity focused ultrasound *Acoust. Phys.* **56** 376–85

Canney M, Khokhlova V, Bessonova O, Bailey M and Crum L 2010 Shock-induced heating and millisecond boiling in gels and tissue due to high intensity focused ultrasound *Ultrasound Med. Biol.* **36** 250–67

Duck F 1990 *Physical Properties of Tissue: a Comprehensive Reference Book* (London: Academic)

Eranki A *et al* 2017 Boiling histotripsy lesion characterization on a clinical magnetic resonance imaging-guided high intensity focused ultrasound system *PLoS One* **12** e0173867

Hamilton M and Blackstock D 1998 *Nonlinear Acoustics* (London: Academic)
Hoogenboom M, Eikelenboom D, den Brok M H, Heerschap A, Futterer J J and Adema G J 2015 Mechanical high-intensity focused ultrasound destruction of soft tissue: working mechanisms and physiologic effects *Ultrasound Med. Biol.* **41** 1500–17
Hu Z, Yang X Y, Liu Y, Sankin G N, Pua E C, Morse M A, Lyerly H K, Clay T M and Zhong P 2007 Investigation of HIFU-induced anti-tumor immunity in a murine tumor model *J. Transl. Med.* **5**
Ishihara Y, Calderon A, Watanabe H, Okamoto K, Suzuki Y, Kuroda K and Suzuki Y 1995 A precise and fast temperature mapping using water proton chemical shift *Magn. Reson. Med.* **34** 814–23
Khokhlova T D, Canney M S, Khokhlova V A, Sapozhnikov O A, Crum L A and Bailey M R 2011 Controlled tissue emulsification produced by high intensity focused ultrasound shock waves and millisecond boiling *J. Acoust. Soc. Am.* **130** 3498–510
Khokhlova V A, Schade G R, Khokhlova T D, Maxwell A D, Sapozhnikov O A, Tsysar S A, Khesuani Y D, Mironov V A and Wang Y N 2017a The use of high intensity focused ultrasound for targeted tissue decellularization *in vivo 2017 Int. Conf. on Biofabrication (Beijing, China, 15–18 October 2017)*
Khokhlova T D, Monsky W L, Haider Y A, Maxwell A D, Wang Y N and Matula T J 2016 Histotripsy liquefaction of large hematomas *Ultrasound Med. Biol.* **42** 1491–8
Khokhlova T D, Wang Y N, Simon J C, Cunitz B W, Starr F, Paun M, Crum L A, Bailey M R and Khokhlova V A 2014 Ultrasound-guided tissue fractionation by high intensity focused ultrasound in an *in vivo* porcine liver model *Proc. Natl Acad. Sci. USA* **111** 8161–6
Khokhlova T D, Haider Y A, Maxwell A D, Kreider W, Bailey M R and Khokhlova V A 2017b Dependence of boiling histotripsy treatment efficiency on HIFU frequency and focal pressure levels *Ultrasound Med Biol.* **43** 1975–85
Khokhlova V A *et al* 2015 Histotripsy methods in mechanical disintegration of tissue: towards clinical applications *Int. J. Hyperthermia* **31** 145–62
Kreider W, Yuldashev P V, Sapozhnikov O A, Farr N, Partanen A, Bailey M R and Khokhlova V A 2013 Characterization of a multi-element clinical HIFU system using acoustic holography and nonlinear modeling *IEEE Trans. Ultrason. Ferroelectr. Freq. Control* **60** 1683–98
Lake A M, Hall T L, Kieran K, Fowlkes J B, Cain C A and Roberts W W 2008a Histotripsy: minimally invasive technology for prostatic tissue ablation in an *in vivo* canine model *Urology* **72** 682–6
Lake A M, Xu Z, Wilkinson J E, Cain C A and Roberts W W 2008b Renal ablation by histotripsy—does it spare the collecting system? *J. Urol.* **179** 1150–4
Maxwell A, Sapozhnikov O, Bailey M, Crum L, Xu Z, Fowlkes B, Cain C and Khokhlova V 2012 Disintegration of tissue using high intensity focused ultrasound: two approaches that utilize shock waves *Acoust. Today* **8** 24–36
Pahk K J, Mohammad G H, Malago M, Saffari N and Dhar D K 2016 A novel approach to ultrasound-mediated tissue decellularization and intra-hepatic cell delivery in rats *Ultrasound Med. Biol.* **42** 1958–67
Reynolds E S 1963 The use of lead citrate at high pH as an electron-opaque stain in electron microscopy *J. Cell Biol.* **17** 208–12
Schade G R, Hall T L and Roberts W W 2012 Urethral-sparing histotripsy of the prostate in a canine model *Urology* **80** 730–5
Simon J C, Sapozhnikov O A, Khokhlova V A, Wang Y N, Crum L A and Bailey M R 2012 Ultrasonic atomization of tissue and its role in tissue fractionation by high intensity focused ultrasound *Phys. Med. Biol.* **57** 8061–78
Styn N R, Wheat J C, Hall T L and Roberts W W 2010 Histotripsy of VX-2 tumor implanted in a renal rabbit model *J. Endourol.* **24** 1145–50
Vlaisavljevich E, Kim Y, Allen S, Owens G, Pelletier S, Cain C, Ives K and Xu Z 2013 Image-guided non-invasive ultrasound liver ablation using histotripsy: feasibility study in an *in vivo* porcine model *Ultrasound Med. Biol.* **39** 1398–409
Vlaisavljevich E, Kim Y, Owens G, Roberts W, Cain C and Xu Z 2014 Effects of tissue mechanical properties on susceptibility to histotripsy-induced tissue damage *Phys. Med. Biol.* **59** 253–70
Vlaisavljevich E, Xu Z, Arvidson A, Jin L, Roberts W and Cain C 2015 Effects of thermal preconditioning on tissue susceptibility to histotripsy *Ultrasound Med. Biol.* **41** 2938–54
Vlaisavljevich E *et al* 2016 Effects of temperature on the histotripsy intrinsic threshold for cavitation *IEEE Trans. Ultrason. Ferroelectr. Freq. Control.* **63** 1064–77
Wang Y N, Khokhlova T, Bailey M, Hwang J H and Khokhlova V 2013 Histological and biochemical analysis of mechanical and thermal bioeffects in boiling histotripsy lesions induced by high intensity focused ultrasound *Ultrasound Med. Biol.* **39** 424–38